Applied Catalysis B: Environmental 132–133 (2013) 389–400

Contents lists available at SciVerse ScienceDirect

Applied Catalysis B: Environmental

journal homepage: www.elsevier.com/locate/apcatb

A search for alternative Deacon catalysts

Markus Hammes, Martin Valtchev, Marion B. Roth, Klaus Stöwe, Wilhelm F. Maier*

Lehrstuhl für Technische Chemie, Saarland University, Saarbrücken, Germany

ARTICLE INFO

Article history:
Received 9 July 2012
Received in revised form
22 November 2012
Accepted 23 November 2012
Available online 1 December 2012

Keywords:
Deacon catalyst
Chlorine Production
Catalyst stability
Catalyst corrosion
High throughput
Emissivity corrected IR-thermography

ABSTRACT

High-throughput methods, emissivity-corrected infrared thermography (ecIRT) and a sequential 10-fold fixed bed gas phase reactor have been used to accelerate the development of new catalysts for the Deacon process ($4\,HCl + O_2 \rightleftharpoons 2\,Cl_2 + 2\,H_2O$). Both setups were modified to withstand the corrosive process conditions. Besides the reactor equipment also the catalysts themselves often suffered corrosion during the reaction. To consider the catalyst corrosion the tested oxides were typically aged for 24 h under a HCl-O_2 atmosphere at reaction temperature. The experimentally observed stability of selected binary mixed-metal oxides is correlated with literature data for the bulk chlorination tendency of the pure oxides and the corresponding melting/sublimation point of the chloride. The starting binary mixed-metal oxides have been selected based on a set of thermodynamic data for bulk chlorination and chloride oxidation and doping of TiO_2 and SnO_2, which are preferentially used as catalyst supports in Deacon reactions. The best catalysts discovered were optimized through doping and composition variations. Characterization of the best materials is provided.

1. Introduction

Chlorine is one of the most important chemical elements in the production of numerous objects for our high standard of living, either directly as component but more often latently in production intermediates; hence the Cl_2 production is an indicator of the development status of a country's chemical industry [1]. However, the production of one ton of Cl_2 by the current membrane chlor-alkali electrolysis needs 2790 kWh electric power equivalent to around 2.1 tons CO_2 [2]. Due to the present energy crisis and increasing concern about anthropogenic CO_2 emissions contributing to the global warming, the huge energy consumption of this process becomes even more important [3]. Apart from technology improvements as by the development of the oxygen depolarized cathode (ODC) [4], the recovery of Cl_2 from the by-product HCl is one piece in the puzzle for more efficient Cl_2 industry, e.g. in the manufacture of isocyanates as intermediates for polyurethanes [3]. The recycling of HCl by electrolysis saves one third of energy compared to the chlor-alkali electrolysis [5,6]. The most efficient way to generate Cl_2 from HCl is the Deacon process. This gas phase process, today based on heterogeneous RuO_2 catalysts, needs only 20% of the energy needed for HCl-electrolysis [7].

The Deacon process was invented and patented by Henry Deacon in 1868. He used Cu compounds on clay as catalysts for the oxidation of gaseous HCl to Cl_2 [8]. The intrinsic problem of Cu based Deacon catalysts is their tendency to evaporate in the presence of chlorine. In 1915, Neumann reported that the undesired catalyst vaporization during the reaction can be reduced by the substitution of Na^+ or K^+ ions into $CuCl_2$ [9]. The original Deacon catalyst has been systematically studied and refined by Shell in the 1960s [10]. In these studies the highest stability and Cl_2 production showed a catalyst composed of 5 wt% Cu, 5 wt% rare earth metal (preferential is a mixture of Pr and Nd) and 3.1 wt% K on a silica support. Further progress in the HCl oxidation has been reported by Mitsui Chemical [11] with a Cr_2O_3 on SiO_2 catalyst in a fluidized-bed reactor (MT-process). This Cr based catalyst is more stable and more active than the Cu based ones. However, there is concern about the release of hazardous Cr(VI)compounds, which is supported by the findings of Amrute et al. [12]. With the discovery of RuO_2 on rutile TiO_2 as long term stable and highly efficient Deacon catalyst by Sumitomo [13], new interest in the research for heterogeneous HCl oxidation catalysts was triggered. Recently Bayer developed Ru based catalysts on cassiterite SnO_2 for this process [14–16]. Both supports, TiO_2 and SnO_2, have the rutile structure in common. This crystal structure favors the epitaxial growth of RuO_2 on the support and is considered a requirement for a high Cl_2 yield [17,18]. Zweidinger et al. have shown that during the catalysis only the surface of RuO_2 is chlorinated and that the process is self-regulating, which is assumed to explain the impressive stability [19]. Furthermore, Sumitomo and Bayer added SiO_2 or γ-Al_2O_3 to their commercial Ru catalysts. These additives reduce agglomeration of the active phase and enhance the long term stability [17,20]. For a deeper understanding of the atomic scale of the Deacon process reviews by Pérez-Ramírez et al. and Over [3,21]

* Corresponding author.
E-mail address: w.f.maier@mx.uni-saarland.de (W.F. Maier).

0926-3373/$ – see front matter © 2012 Elsevier B.V. All rights reserved.
http://dx.doi.org/10.1016/j.apcatb.2012.11.034

can be recommended. Mondelli et al. claimed stable copper-based catalysts as an alternative to noble metal (Ru) containing catalysts [22], while Amrute et al. reported noble metal free CeO_2 as suitable catalysts for the Deacon reaction at 430 °C [23].

In the Deacon process the success of the catalyst is closely related to its corrosion resistance. Due to the extraordinarily high and varying commodity price of the metal Ru there is a need for alternative catalyst compositions which are low in Ru content, active and stable under these harsh conditions. Since broad screening by one at a time experimentation is time consuming and costly, high-throughput (HT) methods had to be developed and applied to accelerate screening and testing. This combination of combinatorial chemistry and HT methods is a valuable approach for the discovery of materials under complex reaction conditions [24,25]. In our search we applied (1) emissivity corrected IR-thermography (ecIRT) for primary screening and (2) a sequential 10-fold gas phase reactor setup with online mass spectrometry for secondary screening. Our ecIRT setup offers possibilities for the testing of up to 206 catalysts in parallel under identical reaction conditions. EcIRT relies on the spatial resolution of small temperature changes, which can be associated to heats of reaction [26]. However, competitive or parallel reactions, such as side-reactions of the catalyst with feed gases or change of emissivity due to reaction of the catalyst surface with feed gas components may hamper the interpretation of the measurement results [27]. More reliable data can be obtained by analysis of the product gas. Such an analysis has been implied in our sequential 10-fold gas phase reactor setup by online mass spectrometry. However this approach reduces the sample throughput strikingly, especially when long-time aging experiments are performed.

Herein we report the results of our HT search for new Deacon catalysts with a focus on stable catalysts compositions.

2. Experimental

2.1. High-throughput syntheses of catalyst libraries

The design of the catalyst libraries were compiled by the in-house software "Plattenbau" [28]. Besides the arrangement of the materials on the slate library, the program calculates all needed volumes of reactants for the material syntheses by the parameterized sol-gel recipes. Finally a pipetting list is created, which is transferred to the pipetting robot.

A commercial pipetting robot (Multiprobe II ex, PerkinElmer) was used for the syntheses. The precursor stock solutions in 5 mL or 10 mL vials were placed on the desktop of the robot. With the help of four pipetting needles the reactants were transferred to 2 mL vials (typical HPLC vials) arranged in racks of 50 vials each.

In the preparation of the catalyst libraries three different composition tolerant acid sol-gel recipes were applied in this study: (1) alkoxide route, (2) propionic acid route and (3) ethylene glycol route. Typically 350 μmol of each material were synthesized in the HT syntheses. Depending on the sol-gel recipe different metal precursors, solvents and complexing agents were used. Commonly 0.1 M alcoholic solutions of nitrates (Ag, Al, Ca, Ce, Co, Cr, Cu, Dy, Er, Eu, Fe, Ga, Gd, Ho, In, K, La, Li, Lu, Mg, Mn, Na, Nd, Ni, Pr, Sc, Sm, Tb, Tm, Y, Yb, Zn), chlorides (Au, Ba, Hf, Ir, Ru, Sb, Sn, Sr, W), alkoxides (Bi, Mo, Nb, Rb, Ta, Ti, V), acids (B, Se, Te) and dinitrate oxide (Zr) were used as standard doping solutions. The heating rates of the synthesis routes are different, they have been optimized in the past to save time and to provide large surface area materials.

2.1.1. The alkoxide route [29]

Highly diverse doped Ti based mixed-metal oxides were synthesized by the alkoxide route. For example, $Cu_{10}Ti_{90}O_x$ was prepared by pipetting 193 μL isopropyl alcohol, 315 μL Ti(IV) isopropoxide (1 M in isopropyl alcohol) and 350 μL Cu(II) nitrate (0.1 M in methanol) in the described order. After finishing all pipetting steps for 50 samples, the rack was placed in an orbital shaker (Titramax 100, Heidolph) for 1 h. The sols were allowed to gel and dry for 5 d at room temperature and finally calcined at 400 °C for 5 h (heating rate 0.5 °C/min) under static air.

2.1.2. The propionic acid route [30,31]

This method allows the preparation of highly diverse doped Sn oxides. The molar ratio of metal(s):isopropyl alcohol:propionic acid was 1:34:35. For instance, to synthesize $Co_2Sn_{98}O_x$ 24 μL 0.1 M Co(II) nitrate was added to 1.372 mL Sn(IV) acetate (0.25 M in 50:50, v:v, isopropyl alcohol:propionic acid). When all pipetting steps for 50 vessels are finished, the 50 vessel rack was placed an orbital shaker for 1 h. The sols were allowed to gel and dry for 7 d at 40 °C before being calcined under static air at 400 °C for 5 h (heating rate 2 °C/min).

2.1.3. The ethylene glycol route [32]

The ethylene glycol route was used to synthesize the binary composition spreads of the elements Ce, Co, Cr, Cu, Fe, La, Mn, Ni and Zn. The metal nitrates of these nine elements were dissolved in a mixture of ethylene glycol:water (100:54, v:v). The molar syntheses ratio of metal(s):ethylene glycol:H_2O:$HNO_{3(conc)}$ was 1:18:37.5:4. For example, $Co_{50}Ni_{50}O_x$ was synthesized by pipetting 231 μL 0.648 M Co(II) nitrate solution, 231 μL 0.648 M Ni(II) nitrate solution, and 83 μL conc. HNO_3. After finishing all pipetting steps of one rack, the samples were placed in an orbital shaker for 1 h. The thermal treating was carried out under static air for 12 h at 80 °C (heating rate 0.3 °C/min), followed by 60 h at 105 °C (heating rate 0.3 °C/min). Finally, the samples were calcined for 5 h at 400 °C (heating rate 0.1 °C/min).

2.1.4. Library preparation

The catalyst powders obtained by HT syntheses were crushed manually with a glass rod in the flasks and transferred manually into the 206 wells positioned hexagonally on a slate library. In addition, pure RuO_2 (Alfa Aesar) has been placed on the slate library as a reference material for ecIRT experiments. Each material was placed three times on the library to generate redundancy for statistical reasons.

The materials prepared were mixed-metal oxides of unknown oxidation states. Since oxidation states may vary with temperature and oxygen partial pressure during pre-treatment, under reaction conditions and during catalytic oxidation reaction, oxidation states are not specified. The material compositions are identified by the mol% of the metal ions as subscript. For instance $Co_{10}Cr_{90}O_x$ mol% Co oxides and 90 mol% Cr oxides.

2.2. EcIRT setup

Our general ecIRT setup for testing 206 catalyst samples in parallel as well as the measurement principles have been reported previously [26,28]. For the screening of catalyst libraries under Deacon conditions the materials of the reactor body and of the reactor periphery were modified. The reactor body as well as the feed lines were manufactured from Inconel 625® or Hastolly C-276®, both nickel super alloys. Furthermore, a corrosion resistant mass flow controller for the dosing of HCl was used. Feed gas quality was 2.8 for HCl (Gerling, Holz & Co), 4.5 for O_2 (Praxair) and 4.5 for N_2 (Westfalen Gas). To prevent corrosion through humidity in the gas supply and reactor setup the whole system was generally purged with N_2 dried over a molecular sieve cartridge placed directly before the gas entering the feedgas line. The corrosive products were removed

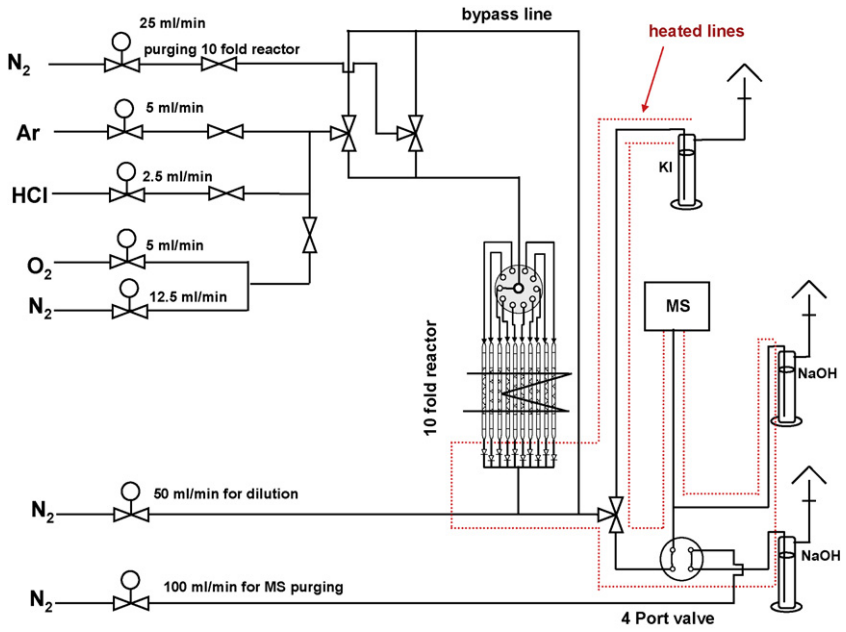

Fig. 1. Scheme of the sequential 10-fold reactor setup.

from the product gas by passing it through caustic soda solution at the outlet of the reactor.

The catalyst library was placed in the centre of the gas phase reactor containing an IR transparent sapphire window on the top. The feed gas enters the reactor from the outer rim simultaneously through 96 small holes equidistantly arranged on the circumference of the reactor wall and the gas flowed from the outside of the library to the gas outlet hole in the centre of the library and the reactor. For *in-situ* observation of temperature changes on the surfaces of the catalyst beds the library was monitored by an IR camera of type PtSi 640 (Thermosensorik). The experimental procedure including temperature regulation, gas dosing and camera setting, was controlled by the in-house software "IR-Testrig". The catalyst library was heated after starting the measurement sequence to the reaction temperature in a N_2 atmosphere. The six point temperature calibration, was carried out under N_2 in a ΔT range of −4 °C to +6 °C around the reaction temperature. Before the start of the chemical reaction, one "IR image", meaning. the accumulation over 1000 individual frames, was taken under the calibration atmosphere as background. Then the feed gas was changed to $HCl:O_2:N_2 = 1:2:7$. During the reaction IR images were taken after 5 min, 10 min, 30 min and 60 min time on stream. After reaction the reactor was again flushed with pure N_2 for 15 min, one additional IR image was taken to document possible emissivity changes of the materials due to bulk chlorination. In addition to the three ΔT values (each sample was present three times on the library), the average and standard deviation were calculated for each material.

The aging produce in the ecIRT reactor was carried out over a 6 h period under reaction conditions, but without recording IR images during the aging. After 6 h the reactor was cooled down first. Then the gas outlet was checked for plugging and often the sapphire window had to be cleaned due to various depositions. Subsequently the samples were examined once more by ecIRT using the standard procedure as described above.

2.3. Conventional syntheses for 10-fold plug flow reactor setup

All materials for the testing in the 10-fold reactor were prepared manually in a batch size of 1 mmol.

2.3.1. The ethylene glycol route [32]

The Cu, Cr or Ru doped Ce, Co and Ni oxides were prepared by the ethylene glycol route as described above in detail. The syntheses were scaled up without changing the thermal treatment and were carried out in 20 mL glass beakers.

2.3.2. The propionate route [33]

For the optimization of the Ru–Co catalysts the propionate method was used. The molar ratio of metal(s):complexing agent: ethanol was 1:3:30. For example, $Ti_2Ru_5Co_{93}O_x$ was synthesized by fully automated pipetting first 2.57 mL ethanol, 0.75 mL 4-hydoxy-4-methyl-pentanon, 1.86 mL 1 M Co(II) propionate (in ethanol), 1.00 mL 0.1 M Ru(III) chloride (in ethanol) and 0.1 M Ti(IV) isopropoxide (in i-propanol) in the described order. The samples were mixed for 1 h and subsequently aged for 7 d at 40 °C. The calcination was carried out under static air for 10 h at 80 °C (heating rate 0.5 °C/min) followed by 5 h at 400 °C (heating rate 0.5 °C/min).

2.4. Sequential 10-fold reactor setup for activity testing

The catalytic testing was carried out in a sequential 10-fold fixed bed reactor setup (see Fig. 1). The setup consisted of the three parts: gas delivery system, 10-fold reactor and quadrupol mass spectrometer (MS). The different feed gases and N2, dried over molecular sieve and added for dilution and flushing, were controlled by mass flow controllers. A 10-port selector valve switched the gases between each plug flow reactor. A 4-port 2-position valve controlled the sample injection into the MS by switching between process gases and flushing N_2. The 10 glass reactor tubes (inner diameter 3.0 mm) were placed equidistant in a circle in an aluminum block around a central heating cartridge to assure a uniform temperature distribution. The process gases were collected in a self-made unit of pressure relief valve system, which avoided the back mixing of the gases between the separate channels. The whole system was manufactured by our machine shop from Inconel® alloy and heated to 110 °C. All lines and valves after the reactor outlets were also heated to the same temperature to prevent water condensation. The valves, mass flow and temperature controllers were controlled by LabView [34], so the testing produce is automated. More details will be published soon.

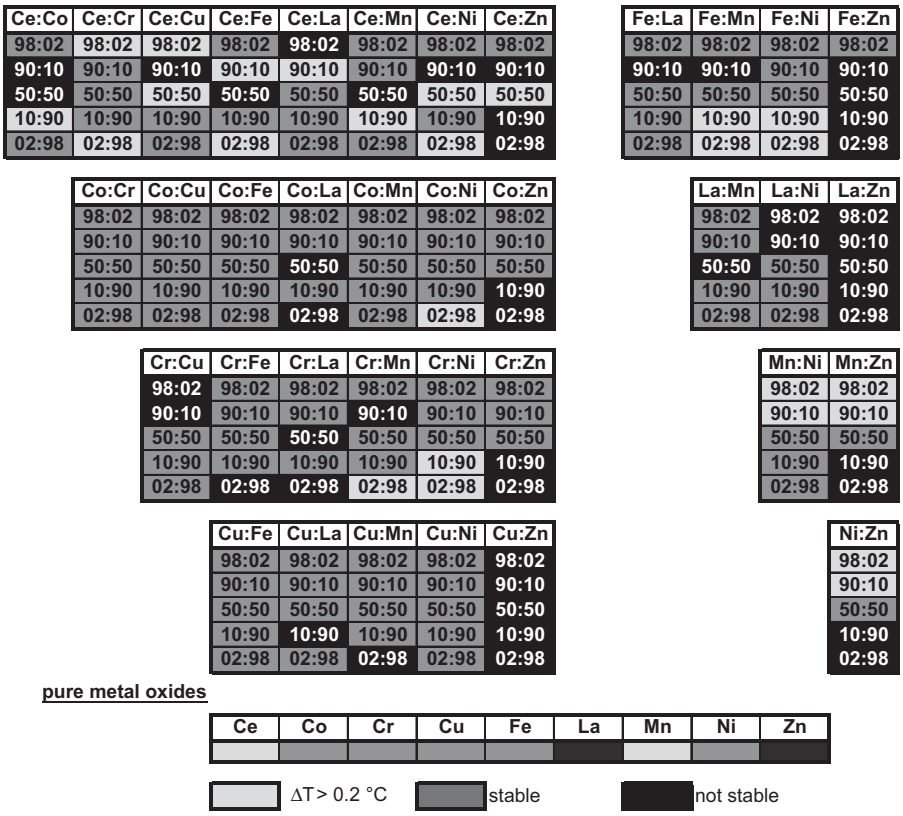

Fig. 2. Overview of the catalyst leaching for the binary mixed-metal oxides consisting of Ce, Co, Cr, Fe, La, Mn, Ni and Zn at 300 °C, feed $HCl:O_2:N_2 = 1:2:7$, as concluded from the ecIRT data.

For the tests, each fixed bed reactor was filled with 37.5 mg catalyst (sieve fraction 100–200 μm) and diluted with 75 or 150 mg quartz sand (sieve fraction 200–300 μm). The samples were heated in N_2 up to the reaction temperature. The composition of the feed gas mixture was $HCl:O_2:Ar:N_2 = 1:2:2:5$ at a WHSV = 40,000 mL/(gh). The analysis of the process gases was carried out by a quadrupole mass spectrometer QMA 200 from Pfeifer Vacuum. The inlet capillary for the MS was a fused silica capillary with an inner diameter of 75 μm and 1.5 m length. The capillary and the vacuum chamber were continuously heated to 110 °C. Every 20 min the process gas was sampled with a pulse duration of 30 s. The device was flushed in the remaining time with N_2 in order to limit the chemical stress for the yttrium oxide coated iridium filament of the ion source. The integrated pulses of the HCl and Cl_2 ion currents were used to calculate the conversion in relation to the bypass. Argon was used as internal standard.

Since the ion currents varied due to the constant corrosion of the filament, the non-linear relationship ion current (M/Z = 36) and the amount of HCl, an additional reference catalyst was used during each run. The conversions of the samples normalized to the reference catalyst (X_n = normalized HCl conversion) allowed the comparison of samples over different runs. As reference catalyst for validation a 2 wt% Ru on SnO_2 stabilized with γ-Al_2O_3 (BMS-reference catalyst) was used. This catalyst, which was supplied by Bayer Material Science, is a well known highly active and stable Deacon catalyst.

To validate the data of the multi-reactor setup the space-time yield (STY) was determined by iodometric titration. This was carried out with a potentiometric titrator 888 Titrando from Metrohm. The samples were taken manually. Typically, the process gases were passed through 100 mL 0.1 M KI solution for a pre-defined time (1–4 min). A 25 mL sample of the resulting solution was titrated with 0.01 M $Na_2S_2O_3$ solution.

2.5. Catalyst characterization

Nitrogen physisorption measurements were performed on a Carlo Erba Sorptomatic 1990 at $T = -196$ °C. The samples were evacuated for 2 h at 200 °C with a heating rate of 5 °C/h. Powder X-ray diffraction (PXRD) pattern were obtained using a PANalytical X'pert Pro MPD (Multi Purpose X-ray Diffractometer) with Ni-filtered Cu radiation ($\lambda(CuK_\alpha) = 1.5418$ Å) in reflection mode. For the Co samples the PHD (Pulse Height Discrimination) lower level of the PIXcel detector was raised from 20% (standard) to 50% to discriminate the Co fluorescence. Crystal data as lattice parameters and Lorentz crystallite sizes were determined by full profile Rietveld refinement using the TOPAS software [35].

3. Results and discussion

3.1. High-throughput and conventional experiments of generation 1

Our development strategy for new efficient HCl oxidation catalysts was based on an evolutionary concept of variation and selection. The starting libraries were arranged by considering the thermodynamic data set for bulk chlorination and chloride oxidation published by Hisham and Benson [36]. By combining different metals, whose oxides are stable against chlorination, but promote oxidation due to thermodynamics an optimal catalyst might be found. For this approach the transition metals Cr, Mn, Fe, Co, Ni, Cu, Zn plus the rare earths elements La and Ce have been combined to 180 binary mixed-metal oxides in the molar ratios of 98:2, 90:10, 50:50, 10:90 and 2:98 by use of the composition tolerant ethylene glycol sol-gel recipes. In addition highly diverse doping has been applied to Sn and Ti dioxides. These oxides were selected due to

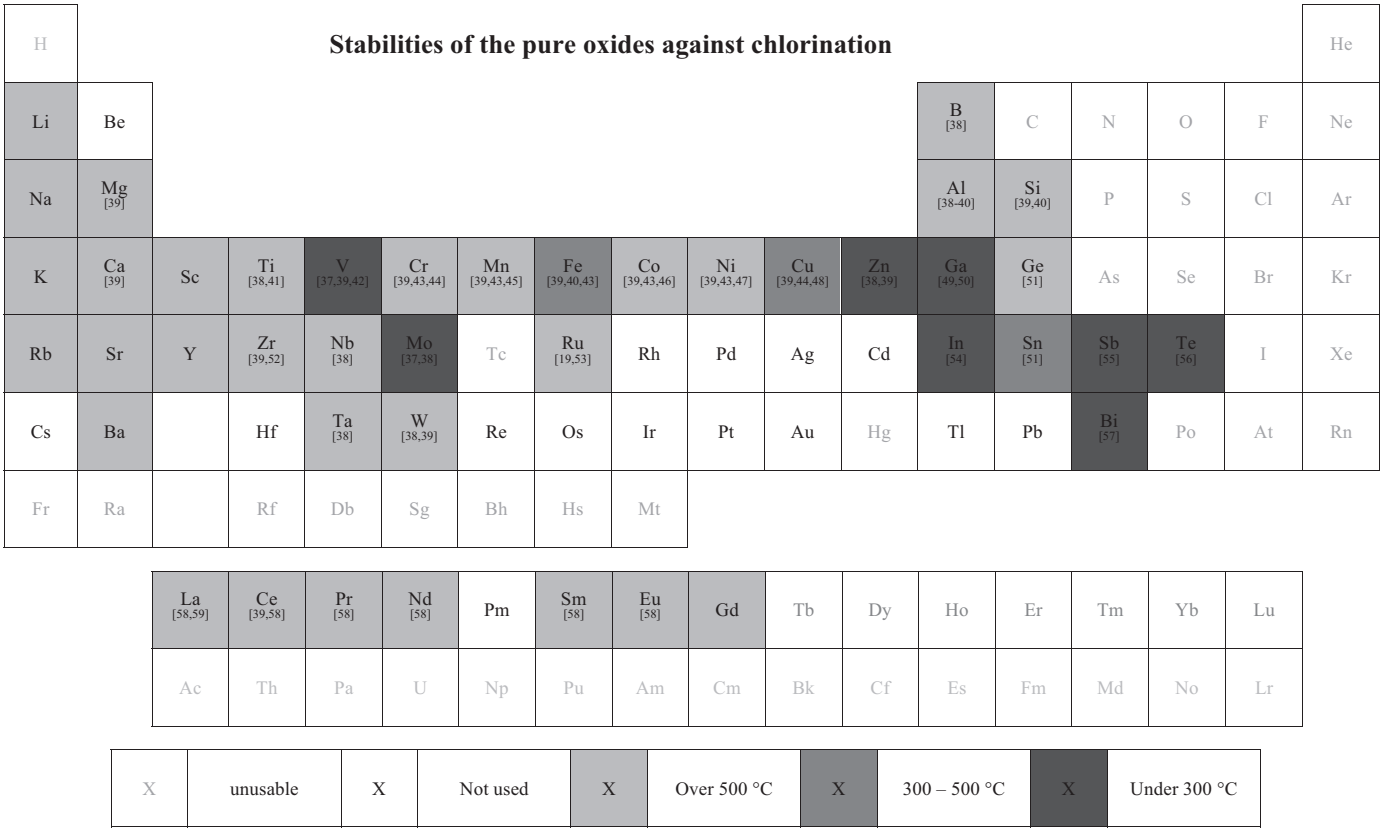

Fig. 3. PSE with stabilities of pure oxides against chlorination. Literature data concerning bulk chlorination of metal oxides, melting/sublimation points and T_4 temperature are combined in this overview.

their potential for forming a rutile structure and their suitability for sol-gel syntheses, low toxicity, and sufficient stability under Deacon conditions. The 50 selected doping elements were: Li, Na, K, Rb, Mg, Ca, Sr, Ba, Ti, Zr, Hf, V, Nb, Ta, Cr, Mo, W, Mn, Re, Fe, Ru, Co, Rh, Ir, Ni, Pd, Pt, Cu, Ag, Au, Zn, B, Al, Ga, In, Si, Ge, Sn, Sb, Bi, Te, Sc, Y, La, Ce, Pr, Nd, Sm, Eu, Gd.

3.1.1. Leaching of mixed-metal oxides under Deacon conditions

For the design of new, heterogeneously catalyzed processes the catalyst life time is a key factor. Especially in the Deacon process many catalysts fail early in the development due to leaching under the corrosive reaction atmosphere. This leaching is caused by chlorination of the metal oxide, which often induces the vaporization of the catalyst components. Besides the type of metal oxide, the chlorination rate depends also on other parameters, such as particle size, feed gas flow and composition. However, our search to find a stable catalyst composition below 400 °C is based on a fixed ratio of $HCl:O_2:N_2 = 1:2:7$ and fixed overall gas flow of 50 mL/min in ecIRT experiments and 25 mL/min in the plug flow reactor thus ignoring the possible influence of the latter two parameters.

Initially the ΔT values from the screening were not ranked, due to the problems of depositions on the sapphire window and catalyst corrosion (see Section 3.1.2). The experimentally observed leaching problems of the binary mixed-metal oxides (Fig. 2) matched with literature data for the chlorination of the pure metal oxides and the melting or sublimation points of their corresponding metal chlorides or oxide chlorides. Apart from the melting und sublimation points the T_4 temperature as introduced by Daniel and Rapp [37] was considered. This temperature describes the point at which the halide vapour pressure attains a value of 10^{-4} atm under static conditions. In Fig. 3 the literature data are combined to visualize the potential of the pure oxides as catalyst for the Deacon process. An oxide is marked as stable, if it is not affected by HCl or Cl_2 below a temperature of 500 °C or the corresponding metal chloride has a low vapour pressure below 500 °C (indicated by a high melting point and T_4 temperature)

From the first screening generation the leaching of 188 materials (180 binary mixed-metal oxides + 8 pure metal oxides) was evaluated visually as relative catalyst loss after 24 h at 300 °C, as shown in Fig. 2. Material compositions that were completely vaporized are marked by black and stable ones by dark gray background in Fig. 2. In addition, stable catalysts, which have a ΔT higher than 0.2 °C show a heat of reaction and are thus marked by light gray background representing the most promising compositions.

25% of the binary Ce mixed oxides studied volatilize at the conditions selected. Especially doping of Ce rich materials enhances the vaporization compared to pure ceria. However, based on these results no clear trends are obvious. The pure Ce oxide is stable in line with reports that characterize CeO_2 as very resistant against bulk chlorination and suitable for the Deacon reaction [23]. CeO_2 chlorination with HCl starts above 500 °C and with Cl_2 above 800 °C [39,58,60]. The combination of Co and rare earths (Ce and La) enhances the volatility of the catalysts. Even the Co–Zn mixed metal oxides vaporized, although various combinations of Co with Cr, Cu, Fe, Mn and Ni mixed-metal oxides appeared suitable. Co_3O_4 reacted with Cl_2 at temperatures around 350 °C and formed $CoCl_2$ [46]. Kasaoka et al. describe also the formation of $CoCl_2$ from a Co spinel at 500 °C in a gas mixture of $HCl:N_2 = 1:99$ (v/v) [39], although the sublimation of the chloride can be neglected below 600 °C [46]. The measurements of the binary Cr mixed-metal oxides showed, that the doping with Cu or Mn promoted the catalyst vaporization. It could be that in the presence of Cu^{1+}/Cu^{2+} or Mn^{3+}/Mn^{4+} redox pairs the oxidation of Cr^{3+} to Cr^{6+} is enhanced. CrO_3 reacts fast with HCl

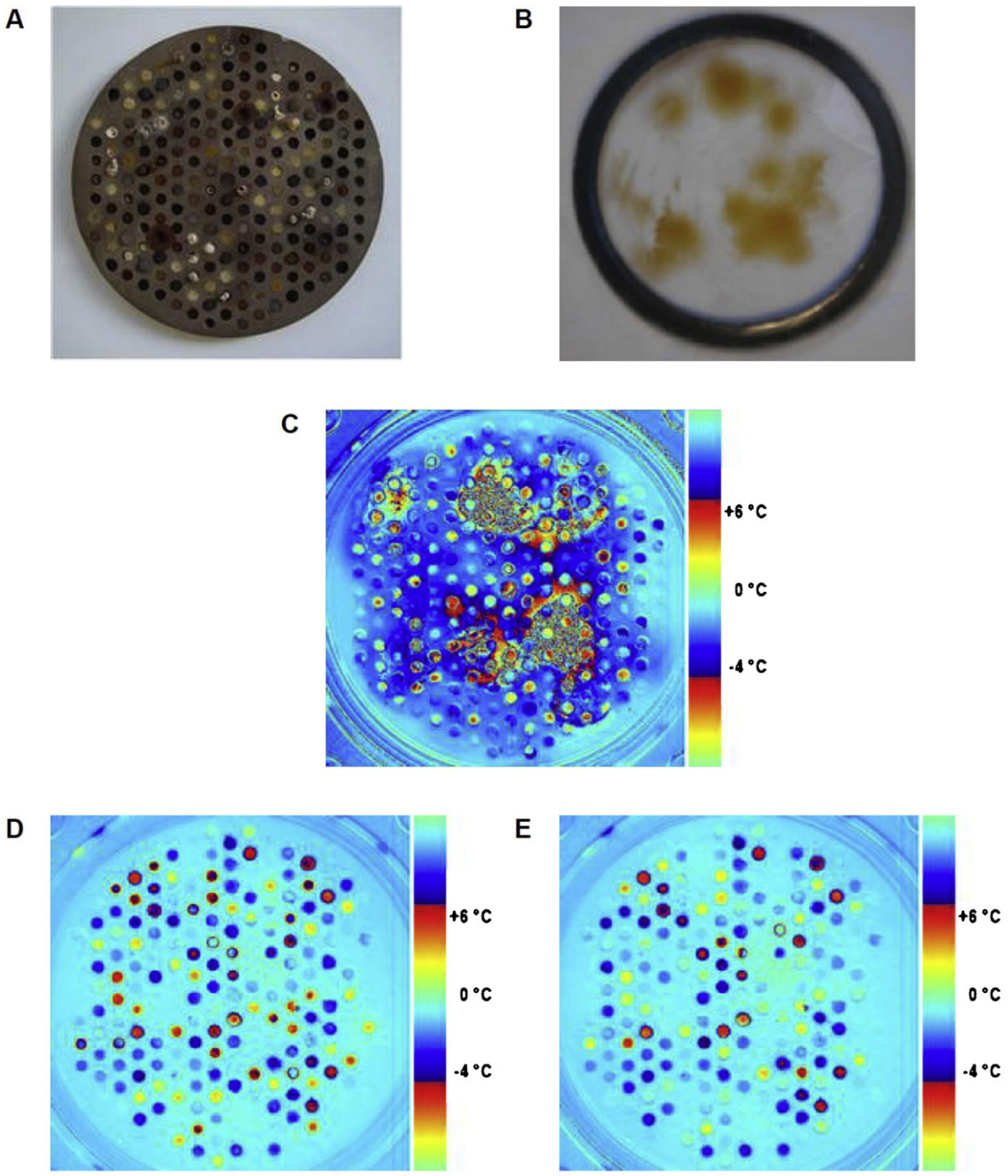

Fig. 4. (A) materials library with Ce, Co, Cr, Cu, Fe, La, Mn, Ni and Zn binary mixed-metal oxides after 24 h Deacon screening at 300 °C (B) depositions on the sapphire window after one aging period of 6 h at 300 °C (C) ecIRT image effected by IR nontransparent depositions on the sapphire window (D) ecIRT image of a materials library after 24 h time on stream under Deacon conditions at 350 °C (E) ecIRT background image of the same materials library after the Deacon reaction under N_2 atmosphere at 350 °C.

to toxic CrO_2Cl_2, which is already volatile at room temperature [61]. For this reason, Cr_2O_3 has to be added continuously to the reaction system. In contrast to this the corrosion resistance of Co–Cr oxides may be explained by the absence of mixed valence Co compounds, because the oxide is reduced directly to $CoCl_2$. In the case of Cu, all Zn containing materials and Cr-rich materials have vaporized at 300 °C as well as Cu oxides doped with 10 mol% Ce or La. Increase of the reaction temperature to 350 °C accelerated the evaporation of Ce–Cu oxides. Cu_2O and CuO are well known to rapidly form CuCl and $CuCl_2$ with HCl and Cl_2 at temperatures below 300 °C [48], which correlates with reports of Amrute et al. and Kasaoka et al., who detected chloride phases after exposure to HCl [39,44]. Problematic is here the CuCl phase, which sublimes in air at 350 °C and has a T_4 temperature of 387 °C [37,62]. All Ce, Cr, La, and Mn doped Fe oxides show clear mass losses after the reaction. At 350 °C and 400 °C even a leaching of Fe chlorides was observed. Fast sublimation of Fe_2O_3 in a HCl stream at 350 °C has been reported by Spitzin [40]. The reasons are the low melting point of 303 °C and a T_4 temperature of 167 °C for $FeCl_3$ [37,62] which apparently forms during the reaction. Interestingly, Kasaoka et al. did not observe chloride formation with Fe_2O_3 below 500 °C in a 1% HCl in N_2 atmosphere. As already observed with the Ce materials, also for La materials

no clear relation between composition and stability was observed. In contrast to CeO_2, La_2O_3 forms LaOCl and $LaCl_3$ at temperatures below 300 °C [58,59]. However, this metal chloride should be stable under reaction conditions due to its melting point of 850 °C. For the manganese oxides MnO (200 °C), MnO_2 (<500 °C), Mn_2O_3 (350 °C) and Mn_3O_4 (450 °C) the formation of metal chlorides below 500 °C is well known [39,43,45]. Melting of $MnCl_2$, which results preferentially under chlorination conditions [45], is reported around 652 °C and the corresponding T_4 temperature is 607 °C. So $MnCl_2$ can be expected to have sufficient stability at reaction conditions. However, Wasmuht reports the loss of manganese during the chlorination of MnO below 500 °C [43]. We have also noticed significant vaporization with the mixed manganese oxides $Ce_{50}Mn_{50}O_x$, $La_{50}Mn_{50}O_x$, $Cr_{90}Mn_{10}O_x$, $Fe_{90}Mn_{10}O_x$ and $Cu_2Mn_{98}O_x$. Most of the Ni oxides were stable under the selected reaction conditions. Exceptions were Ni doped rare earth oxides and Zn-rich mixed oxides. A clear correlation between metal content and stability was found for Zn oxides, i.e. the more Zn content the higher is the vaporization. Over 60% of the Zn oxides have disappeared completely during the Deacon tests. This is in line with the low melting point of $ZnCl_2$ (285 °C). Additionally, highly diverse doped Ti and Sn oxides were tested for the Deacon reaction at different temperatures. For doped Ti oxide no noticeable leaching was observed during our experiments. This is in agreement with the literature. According to these data TiO_2 reacts with HCl at over 600 °C and with Cl_2 at over 800 °C [38,41]. The other important catalyst support in HCl oxidation is Sn oxide, which is known to form $SnCl_4$ around 400 °C [51]. Due to the low boiling point of 114 °C of $SnCl_4$ a fast volatilization of the material can be assumed. In our experiments 380 °C was never exceeded. However, especially for alkaline earth doped Sn oxides a higher material loss was observed than for the other doped oxides. This may be explained by the formation of reactive chlorides, such as $CaCl_2$, which by itself is a strong chlorination agent [63].

3.1.2. Challenges of ecIRT screening due to the Deacon reaction

The exothermic oxidation of HCl with O_2 to Cl_2 and H_2O (ΔH° = -56.8 kJ per mol Cl_2) seemed ideal for the screening by ecIRT, since no exothermic parallel or secondary reactions are likely. Due to the highly corrosive reaction conditions, all parts in contact with the gases in the ecIRT reactor were made from the nickel super alloys Inconel® and Hastelloy®.

During pre-screening experiments with mixed oxide catalysts it was noted that the materials tested were also often affected by these corrosive conditions (see Fig. 4A). Besides the heterogeneously catalyzed HCl oxidation, the exothermic bulk chlorination of the metal oxides is a competitive side reaction, changing catalyst surface and thus emissivity. For a number of binary mixed oxides a vapor transport reaction occurs by the vaporization of the metal chlorides or metal oxide chlorides formed, which often resulted in an undesired vapor deposition on the colder sapphire window (Fig. 4B) or in the reactor exhaust line. Such deposited films are often not transparent for IR radiation and reduce the intensity of the heat signal of the underlying catalyst (Fig. 4C). Also the generated metal oxide chlorides and metal chlorides on the library plate revealed different emissivities than the starting oxides. The emissivities of the starting oxides at the six calibration temperatures was used to adjust the polynomial function for the latter analysis including the determination of the ΔT values [26]. Therefore emissivity changes result in false ΔT values leading to false negatives or false positives. Furthermore, it was sometimes observed that the temperature changes exceeded the calibration range, which resulted in a cycling through the calibration temperature range more than once. This is clarified in the temperature scales given in Fig. 4. One way to deal with such phenomena is to take another IR image several min after reaction (here under N_2 atmosphere) and subtract it from the last reaction image. Fig. 5 shows the plot of the

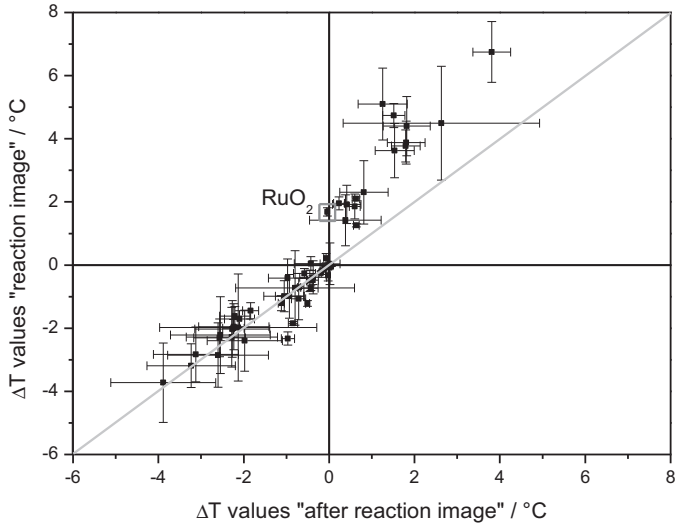

Fig. 5. ΔT values "reaction image" vs. ΔT values "after reaction image" for materials library with Ce, Cr, Co, Cu, Fe, Mn, and Ni binary mixed-metal oxide and RuO_2.

ΔT values "reaction image" (data from Fig. 4D) vs. "after reaction image" (data from Fig. 4E). For negative ΔT values close to the diagonal we conclude, that these materials have been chlorinated and show no catalytic activity. However, those oxides showing positive (exothermic) ΔT values after the subtraction of the "after reaction image", the positive deviation from the diagonal is interpreted as heat of reaction and they were therefore of interest for further studies (regarded as hits).

Depending on the nature of the metal ion and its oxidation state, the chloride formation enthalpies are often comparable to the reaction enthalpy of the HCl oxidation (see Section 3.1.3) [36]. In Fig. 6 the background corrected ΔT values from ecIRT for the chlorination ($HCl:N_2$ = 1:9) and the background corrected ΔT values of Deacon reaction ($HCl:O_2:N_2$ = 1:2:7) at 300 °C are compared. Fig. 6 documents that the bulk chlorination of the tested transition and rare earth mixed-metal oxides strongly affect the ecIRT analysis, which is most likely due to the similar enthalpies of bulk chlorination and Deacon reaction [36]. Only the pure RuO_2 reference and $Ce_{90}Mn_{10}O_x$ have higher ΔT values for the Deacon reaction relative to the chlorination.

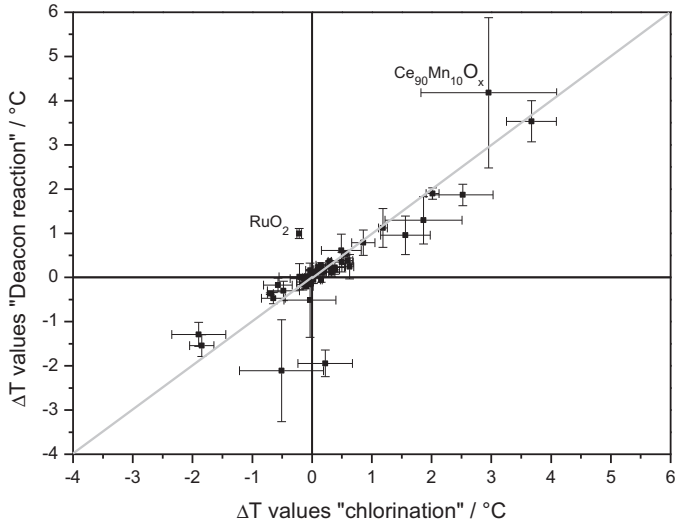

Fig. 6. Plot of ΔT values "Deacon reaction" (feed $HCl:O_2:N_2$ = 1:2:7) versus ΔT values "chlorination" (feed: $HCl:N_2$ = 1:9) both at 300 °C.

Table 1
Normalized HCl conversion X_n after 50 min for the Cr, Cu or Ru doped Ce, Co or Ni oxides at different dopand levels, all values are normalized to the reference catalyst; exp. conditions: temperature 380 °C, flow rate 25 mL/min, gas composition HCl:O_2:Ar:N_2 = 1:2:2:5, catalyst mass 37.5 mg (100–200 μm) + 75 mg quartz sand (200–300 μm); n.X. = no HCl conversion.

Matrix	Cr (mol%)				Cu[a] (mol%)				Ru (mol%)			
	2	5	10	20	2	5	10	20	2	5	10	20
Ce	n. X.	0.05	0.04	0.31	0.08	0.36	0.47	0.40	0.07	0.33	0.32	0.34
Co	0.21	0.60	0.66	0.56	n. X.	n. X.	n. X.	n. X.	0.62	1.10	0.99	0.86
Ni	n. X.	n. X.	0.17	0.27	n. X.	n. X.	n. X.	n. X.	n. X.	n. X.	n. X.	0.59

[a] Depositions in the colder reactor parts.

The error bars given in Fig. 6 and later figures are based on the data obtained on the same library from the same compound on different library positions (usually every compound is placed three times on each library for statistical reasons (see above). The error bars for RuO_2 and $Ce_{90}Mn_{10}O_x$ are different, most likely due to their different reaction behavior under these conditions. In ecIRT often Ce based materials reveal obvious emissivity changes during experiments under oxidizing conditions [27]. The presence of chlorinating compounds enhanced this effect. Especially for $Ce_{90}Mn_{10}O_x$ the difference in the position on the slate plate - comprising also small differences in the gas composition - induced large variations and large emissivity changes. In contrast, RuO_2 is not effected by bulk chlorination and consequently shows no emissivity change. An explanation could be, that on most mixed oxides the Deacon reaction follows a Mars van Krevelen mechanism, which facilitates chlorination [66], while on Ru based catalysts the reaction follows a Langmuir–Hinshelwood mechanism [53].

3.2. High-throughput and conventional experiments of generation 2

Due to the problem with ecIRT of competitive bulk chlorination described above the 2nd generation screening was carried out with the 10-fold reactor setup. The process gases were analyzed online by mass spectrometry (MS). All results of each run in the 10-fold reactor were normalized to the reference catalyst or to the undoped oxide catalyst. The search for better catalysts was continued by doping the stable metal oxides Ce, Co and Ni, selected by results of the primary screening and literature data, with Cr, Cu and Ru ions, all well known for Deacon activity. Additional 21 doping elements, i.e. Al, B, Ca, Ce, Co Ge, Hf, K, La, Mg, Na, Nb, Ni, Sc, Si, Sn, Ta, Ti, W, Y and Zr, have been selected with respect to chlorination properties and melting/sublimation points (see Fig. 3).

3.2.1. Doping of Ce, Co and Ni oxide with Cr, Cu or Ru

The Ce, Co, and Ni oxides doped with 2, 5, 10, 20 mol% of Cr, Cu and Ru were tested at 380 °C. Table 1 summarizes the MS results of the HCl conversion normalized to the BMS reference catalyst. Since with most of the screened materials chlorination occurs in the beginning, HCl conversions have only been considered after 50 min reaction time.

The doped Ni oxides showed the lowest Cl_2 yield of the three doped oxides studied. No Cl_2 formation was detected for Cu–Ni oxides. For the most active Ni catalysts a high degree of doping of at least 10 mol% Cr or 20 mol% Ru was necessary.

In contrast to Ni, for the doped Ce oxides an increase of Cu and Ru doping over 5 mol% did not promote HCl conversion any further, while HCl conversion increased with the Cr loading.

For the Co based catalysts 10 mol% doping with Cr or Ru seemed optimal (see Table 1). $Ru_5Co_{95}O_x$ and $Ru_{10}Co_{90}O_x$ achieved conversions comparable to that of the BMS reference catalyst. XRD investigations revealed for these oxides a dominant spinel crystal phase (see Fig. 7).

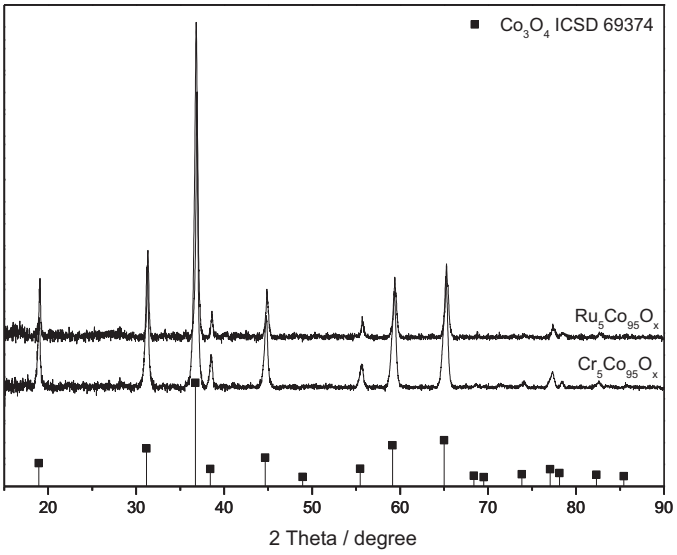

Fig. 7. XRD pattern of $Ru_5Co_{95}O_x$ and $Cr_5Co_{95}O_x$.

Out of the 36 catalysts from Table 1 the nine best ones were selected and the experiments were repeated at T = 350 °C. Subsequently the candidates were aged at 400 °C for 24 h and tested again at 350 °C. All results in Table 2 are normalized to the fresh BMS reference catalyst. Especially for the doped transition metal oxides of Co and Ni chlorination was observed at the beginning of the experiments. For that reason only the conversion rates after 50 min were considered for these oxides (marked with an asterisk in Table 2). In the case of $Cu_{10}Ce_{90}O_x$ and $Ru_{20}Ni_{80}O_x$ a strong deactivation in comparison to the reference catalyst is observed. On the other side the Cr-Co oxides and $Ru_5Co_{95}O_x$ seemed to have a similar aging behavior like the reference, which is indicated by nearly constant X_n before and after aging. An increase of X_n after aging, like for $Ru_{10}Co_{90}O_x$, led to the conclusion, that this catalyst was more stable than the reference. Furthermore, after aging all four doped Ce oxides showed the same normalized HCl conversion around 0.4. So

Table 2
Normalized HCl conversions X_n at T = 350 °C normalized to the reference catalyst. The catalysts were aged at T = 400 °C for t = 24 h at feed composition HCl:O_2:N_2 = 1:2:7 and subsequently tested at T = 350 °C.

Catalyst	X_n (fresh)	X_n (aged)
$Cu_5Ce_{95}O_x$	0.32	0.45
$Cu_{10}Ce_{90}O_x$	0.66	0.36
$Ru_5Ce_{95}O_x$	0.26	0.42
$Ru_{10}Ce_{90}O_x$	0.25	0.39
$Cr_5Co_{95}O_x$	0.60	0.53
$Cr_{10}Co_{90}O_x$	0.79	0.73
$Ru_5Co_{95}O_x$	1.16[a]	1.20[a]
$Ru_{10}Co_{90}O_x$	0.87[a]	1.27
$Ru_{20}Ni_{80}O_x$	0.69[a]	0.51

[a] Due to chlorination of the bulk material only the last measurement point was considered.

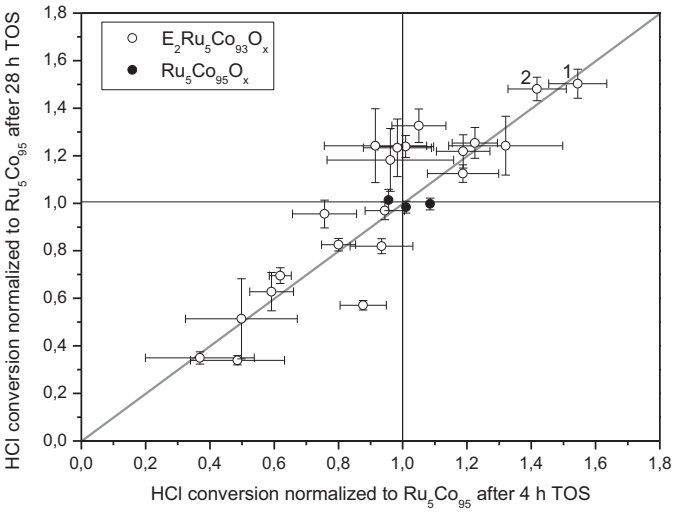

Fig. 8. Conversion plot of doped $Ru_5Co_{95}O_x$ after 4 h time on stream (TOS) vs. 28 h time on stream; the HCl conversions were normalized to the HCl conversion of the undoped catalyst; exp. conditions: temperature 350 °C, flow rate 25 mL min^{-1}, gas composition HCl:O_2:N_2 = 1:2:7, catalyst mass 37.5 mg (100–200 μm) + 150 mg quartz sand (200–300 μm).

neither the element nor the degree of doping seemed to have an effect.

3.2.2. Optimization of $Ru_5Co_{95}O_x$

The optimization of the promising $Ru_5Co_{95}O_x$ catalyst was started by 2 mol% doping with the 20 elements listed above under section 3.2 (Co was excluded). Out of this list Ti, Nb, Ta, Sn, Si, W and Ge could not be used in combination with the ethylene glycol sol-gel recipe. Therefore the synthesis was changed to the propionate route, which is tolerant for all selected doping elements. Through the change of synthesis a drop of catalyst activity from X_n = 1.10 (ethylene glycol) to X_n = 0.80 (propionate) was observed relative to the reference catalyst. The testing of all 20 catalysts together with the undoped one and the reference catalyst resulted in three complete runs with the 10-fold reactor setup. A complete run is composed of the following steps: the HCl conversion was first tested after 4 h on stream and normalized to the undoped $Ru_5Co_{95}O_x$. Subsequently the catalysts were aged for 24 h at 400 °C under Deacon conditions and screened again at 350 °C. In Fig. 8 the normalized HCl conversions of the doped Ru-Co catalysts after 4 h are plotted against those of the aged catalysts after 28 h. Most of the catalysts match the angle bisector indicating that during the reaction time range applied the catalysts were neither deactivated nor activated. However doping the Ru–Co mixed-metal oxides with Ca, Ce, Mg, Ti or Sc increased the HCl conversion with time. The best catalysts after 28 h were $Al_2Ru_5Co_{93}O_x$ (1 in Fig. 8, $X_n = 1.50 \pm 0.06$) and $Zr_2Ru_5Co_{93}O_x$ (2 in Fig. 8, $X_n = 1.48 \pm 0.05$).

Variation of the amount of Al or Zr (see Table 3) revealed that there was little effect of the Al content and an optimal amount of 2 mol% of Zr for HCl conversion activity was found.

The X_n of $Zr_2Ru_5Co_{93}O_x$ was also compared with state of the art Deacon catalysts Ru on TiO_2(rutile) and Ru on SnO_2(cassiterite). For reasons of better comparison, all catalysts were prepared by sol–gel synthesis and all samples contained the same amount of Ru (5 mol%). At 350 °C $Ru_5Ti_{95}O_x$ had only a X_n = 0.62. The reasons for the low X_n might by that the TiO_2 part consisted of a rutile and anatase phase mixture (phase analyses is not shown here). The other two catalysts exhibited a high X_n of 1.47 for $Ru_5Sn_{95}O_x$ and 1.54/1.48 for $Zr_2Ru_5Co_{93}O_x$. For both catalysts the normalization factors to the supplied reference catalyst were higher than one. This indicates, that the performance of the sol-gel catalysts are better than the performances of the reference catalyst, prepared by impregnation. The STY for $Ru_5Co_{95}O_x$ and $Zr_2Ru_5Co_{93}O_x$ catalysts was controlled after 1 h, 24 h and 100 h time on stream (see Table 4). Independent of time the Zr doped catalyst showed an improved activity over the undoped catalyst of a factor of 1.4. The Cl_2 production of both catalysts was constant during the first 24 h and slowly decreased thereafter. Nevertheless $Ru_5Co_{95}O_x$ and $Zr_2Ru_5Co_{93}O_x$ were very stable Deacon catalysts.

Before studying the light-off behavior of the new catalysts the experimental conditions were optimized. In the case of the screening experiments the catalytic activity of the Zr–Ru-Co mixed-oxides was found to be slightly limited by mass transport phenomena. This mass transport limitation could be overcome by increasing the volume flow rate from 25 mL/min to 50 mL/min while keeping the contact time constant. Due to the similar BET surface areas (see Table 5) the direct comparison of catalyst performances with that of the reference catalyst seemed acceptable. Fig. 9 represents the light-off curves obtained. The upper line in Fig. 9 marks the equilibrium limitation for HCl conversion with temperature; it was calculated by the data from Arnold and Kobe for the gas composition HCl:O_2:N_2 = 1:2:7 [64]. Particularly at temperatures lower than 350 °C the new Zr doped Ru-Co catalyst showed superior properties. $Zr_2Ru_5Co_{93}O_x$ converted twice the amount of HCl at 260, 290 and 320 °C than the BMS reference. However, at high temperatures of 375–450 °C the reference catalyst is not surpassed. Remarkable was also the difference in the slope of the light-off curves. Especially $Ru_5Co_{95}O_x$ showed a constant increase from 8% at 290 °C to 70% at 440 °C, while the supported reference catalyst showed a much sharper increase of activity between 320 °C and 380 °C.

Table 3
Variation of dopand amount for Al and Zr in $M_yRu_5Co_{95-y}O_x$; HCl conversion was normalized to the HCl conversion of the undoped catalyst; exp. conditions: temperature 350 °C, flow rate 25 mL/min, gas composition HCl:O_2:N_2 = 1:2:7, catalyst mass 37.5 mg (100–200 μm) + 150 mg quartz sand (200–300 μm).

Catalyst	X_n (fresh)	X_n (aged)
$Al_1Ru_5Co_{94}O_x$	1.47 ± 0.26	1.35 ± 0.14
$Al_2Ru_5Co_{93}O_x$	1.59 ± 0.29	1.39 ± 0.15
$Al_4Ru_5Co_{91}O_x$	1.66 ± 0.28	1.38 ± 0.13
$Zr_1Ru_5Co_{94}O_x$	0.83 ± 0.17	1.19 ± 0.12
$Zr_2Ru_5Co_{93}O_x$	1.54 ± 0.25	1.75 ± 0.17
$Zr_4Ru_5Co_{91}O_x$	1.18 ± 0.20	1.51 ± 0.15
$Ru_5Co_{95}O_x$	1.00 ± 0.10	1.00 ± 0.03

Table 4
STY of $M_yRu_5Co_{95-y}O_x$ (M = Zr, y = 0, 2) after several hours given in g(Cl_2)/h/g(catalyst); exp. conditions: temperature 350 °C, flow rate 25 mL/min, gas composition HCl:O_2:N_2 = 1:2:7, catalyst mass 37.5 mg (100–200 μm) + 150 mg sphere glass (>500 μm).

Catalyst	Fresh	24 h (*28 h)	100 h
$Ru_5Co_{95}O_x$	2.3	2.5	2.1
$Zr_2Ru_5Co_{93}O_x$	3.3	3.4*	3.0

Table 5
BET surface and pore radius (pore radius determined by BJH method). A and B are different synthetic batches.

Catalyst	BET surface area (m^2/g)	Mean pore radius (nm)	Max pore radius (nm)
$Co_{100}O_x$	33	7.48	7.56
$Ru_5Co_{95}O_x$ (A)	28	7.94	2.06
$Ru_5Co_{95}O_x$ (B)	19	10.04	1.94
$Zr_2Ru_5Co_{93}O_x$ (A)	37	6.80	2.04
$Zr_2Ru_5Co_{93}O_x$ (B)	32	6.16	2.12
Reference catalyst	32	6.69	4.89

Table 6
Lattice parameters as well as crystallite sizes related to cubic Co_3O_4 (ICSD 69374) after preparation and after 100 h Deacon reaction at 350 °C. Given in parentheses are the standard deviations for the last indicated number.

Catalyst	After preparation		After Deacon		
	a (Å)	Crystallite size L in nm	Fraction Co_3O_4	*a* (Å)	Crystallite size L in nm
$Co_{100}O_x$	8.079 (1)	33 (1)	15%	8.085 (1)	61 (3)
$Zr_2Co_{98}O_x$	8.076 (2)	18 (1)	<1%		
$Ru_5Co_{95}O_x$	8.083 (1)	60 (2)	8%	8.089 (1)	54 (3)
$Zr_2Ru_5Co_{93}O_x$	8.083 (1)	53 (2)	10%	8.089 (1)	56 (7)

3.3. Catalyst characterization

The characterization techniques N_2 adsorption and XRD were applied to address the modifications triggered by the doping of Co oxide with Ru and Zr after calcination and after 100 h Deacon reaction. For better comparison a sample of $Co_{100}O_x$ was prepared by the same recipe as the doped mixed oxides.

For heterogeneous catalysts surface area and pore size distribution are essential parameters. In Table 5 the results of the BET surface determination are summarized. All materials have small surface areas, unusual for oxides prepared via a sol-gel synthesis. The modification with Ru leads to a slight decrease of the surface area and the maximum pore size also shifts to lower radii in relation to the undoped oxide. In contrast to this doping with Zr enhanced the BET surface compared to $Co_{100}O_x$. This effect of Zr on surface area was also be observed for $Zr_2Ru_5Co_{93}O_x$ vs. $Ru_5Co_{95}O_x$. Both modifiers Ru and Zr reduce the maximum pore radii.

After preparation the spinel Co_3O_4 (ICSD 69374) was the dominant crystalline phase in all samples (see Fig. 10). No additional crystalline phases could be identified by doping with Ru and Zr. For the $Zr_2Ru_5Co_{93}O_x$ a crystalline tetragonal RuO_2 phase was observed. The formation of RuO_2 with a rutile-type structure by doping the Ru–Co catalyst with Zr seems to correlate with an enhanced HCl conversion. Rietveld refinements were performed to obtain more detailed informations on these crystalline phases. The cubic Co_3O_4 phase has a preferred orientation of [1 1 1] in all samples after synthesis. As shown in Table 6 the lattice parameter *a* as well as crystallite size L were affected by Ru and Zr. Doping the cubic Co_3O_4 with 2 mol% Zr reduces the lattice parameter *a* and decreases the crystallite size L from 33 nm to 18 nm. In contrast, addition of Ru resulted in an increase of the lattice parameter

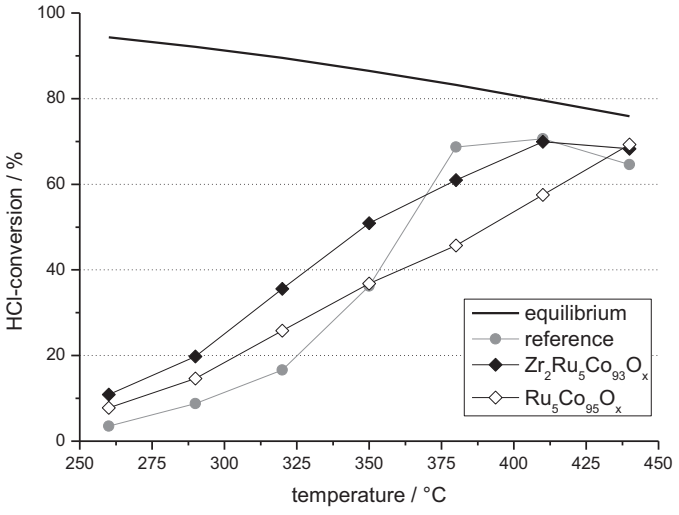

Fig. 9. Light-off curves for $Ru_5Co_{95}O_x$, $Zr_2Ru_5Co_{93}O_x$ and reference; exp. conditions: flow rate 25 mL/min, gas composition $HCl:O_2:N_2 = 1:2:7$, catalyst mass 75 mg + 300 mg quartz sand (both: sieve fractions 100–200 μm).

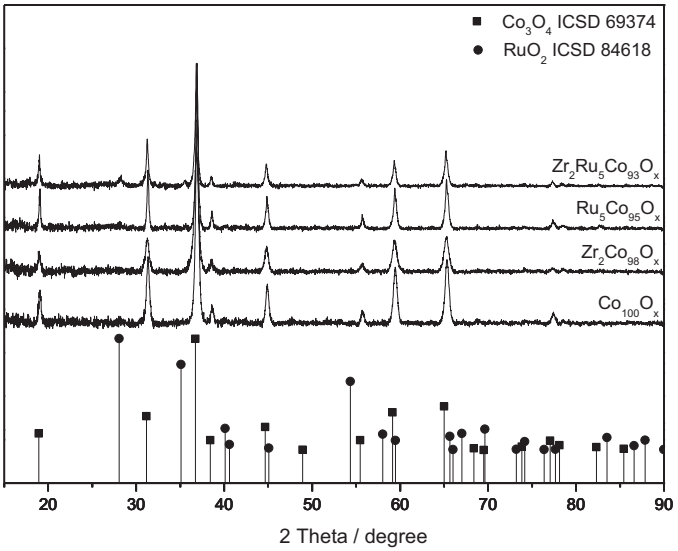

Fig. 10. XRD pattern of doped Co mixed-metal oxides and the undoped cobalt oxide. All samples were prepared by the propionate sol–gel recipe.

(from *a* = 8.079(1) to *a* = 8.083(1) Å) and nearly a doubling of the crystallite size. The growth of lattice parameter *a* is triggered by incorporation of Ru^{3+} into octahedral sites of the spinel. However, this effect is not very distinct, when compared to the reported lattice parameters of *a* = 8.183 Å for $Co_{2.6}Ru_{0.4}O_4$ and *a* = 8.344 Å for Co_2RuO_4 [65], but compared to 5 mol% in these compounds the Ru content was also higher (13.3 and 33 mol%, respectively). From the magnitude of the lattice parameter increase we conclude that not the complete 5 mol% Ru are substituted into the spinel lattice but there might also be the formation of some RuO_2 of low crystallinity or even amorphous structure. For the best catalyst $Zr_2Ru_5Co_{93}O_x$ *a* is identical to the lattice parameter of $Ru_5Co_{95}O_x$, but Zr reduces the crystallite size as in the case of Co_3O_4. After 100 h at 350 °C with $HCl:O_2:N_2 = 1:2:7$ feed gas most of the Co spinel was converted into $CoCl_2 \cdot 2\,H_2O$. No spinel was found for $Zr_2Co_{98}O_x$. The rutile phase of RuO_2 was still present in the $Zr_2Ru_5Co_{93}O_x$ sample after the Deacon reaction. For the spinels the lattice parameters have increased, but the effect of Ru doping was still observable.

4. Conclusion

In this study two different high-throughput technologies, ecIRT and a 10-fold gas phase flow reactor, have been applied to screen for new catalysts as well as optimize the most promising candidates for the Deacon reaction. Initially ecIRT was used to test over 500 materials and served especially as prescreening tool. Besides catalytic activity, corrosion resistance of the binary mixed-metal oxides to the Deacon conditions has been a topic of major concern. We identified a correlation between the literature reports for the bulk chlorination properties of the pure metal oxides and our screening

results for the mixed oxides. Therefore the composition dependent stability of sol-gel based Deacon catalysts can be predicted for each oxide component from literature data of bulk chlorination tendency and melting/sublimation point of the corresponding chloride/oxide chloride in a first approximation. Examples are: binary La or Zn oxides at 300 °C, Cu or Fe mixed-metal oxides above 350 °C.

Two drawbacks of the ecIRT method were identified during the screening: (1) the emissivity of mixed oxide often changed due to bulk chlorination during the reaction. These undesired changes could be corrected for by subtraction of the image after reaction from the last image under reaction. (2) because of the insufficient selectivity of the ecIRT between two reactions with comparable reaction enthalpies, the screening was carried out with two different gas mixtures to distinguish between bulk chlorination and heterogeneous Deacon reaction ($HCl:N_2 = 1:9$ and $HCl:O_2:N_2 = 1:2:7$). The results indicated that the mixed-metal oxides, especially transition metals, are more affected by bulk chlorination than Ru based materials. Therefore ecIRT in this project mainly served to identify problematic catalysts and remove them from the potential hits. The final catalyst optimization and selection was carried out in the sequential 10-fold reactor, in which 60 materials were investigated. The advantage of this setup was, that due to application of online mass spectrometry, a distinction between bulk chlorination and HCl oxidation was possible by recording both the HCl and the Cl_2 ion current signal.

During the screening of the second generation, Ru or Cr doped Co spinel catalysts were identified as potentially active and stable Deacon catalysts. The growth of the lattice constant *a* for the cubic Ru doped Co_3O_4 compared to undoped Co spinel as reference indicates an incorporation of Ru^{3+} in the lattice. The catalyst is mainly converted to $CoCl_2 \cdot 2\ H_2O$ during the long term testing, but the STY is not affected to the same extent and decreases only slightly (most likely because data collection begins only after 50 min, when steady state conditions are reached and surface or bulk chlorinations are finished). This finding for spinel based catalysts shows that there is still potential for new Deacon catalysts besides the favored rutile-type ones, such as RuO_2. It should be emphasized, that all the conclusions based on elemental interactions and compositions apply strictly only to the sol-gel-prepared materials described here. Their extrapolations to any other materials of identical composition, although highly likely, has not been investigated.

Acknowledgement

This work was supported by the Bundesministerium für Bildung und Forschung (BMBF) under contact number 033R018G.

References

[1] R. Bartsch, C.L. Curlin, T.F. Florkiewicz, B. Lüke, H.-R. Minz, T. Navin, R. Scannell, P. Schmittinger, E. Zelfel, in: P. Schmittinger (Ed.), Chlorine, 1st ed., Wiley-VCH Verlag GmbH, Weinheim, 2000.
[2] http://www.eurochlor.org/media/9385/3-2-the_european_chlor-alkali_industry_-_an_electricity_intensive_sector_exposed_to_carbon_leakage.pdf
[3] J. Pérez-Ramírez, C. Mondelli, T. Schmidt, O.F.K. Schluter, A. Wolf, L. Mleczko, T. Dreier, Energy & Environmental Science 4 (2011) 4786–4799.
[4] F. Gestermann, in GDCh - Monographien Band 23: Elektronenübertragung in Chemie und Biochemie, 2001, pp. 137–145.
[5] D. Hoormann, H. Pütter, J. Jörissen, Chemie Ingenieur Technik 77 (2005) 1363–1376.
[6] I. Moussallem, J. Jorissen, U. Kunz, S. Pinnow, T. Turek, Journal of Applied Electrochemistry 38 (2008) 1177–1194.
[7] A. Hiroyuki, U. Youhei, K. Seki, C. Knapp, O. Norihito, K. Masahiro, Sumitomo Kagaku 2010, pp. 1–10.
[8] H. Deacon, U.S. Patent 85,370 (1868).
[9] B. Neuman, Angewandte Chemie 28 (1915) 233–236.
[10] F. Wattimena, W.M.H. Sachtler, Studies in Surface Science and Catalysis 7 (1981) (New Horizons in Catal. Proceedings of the 7th International Congress on Catal.), 816–827.
[11] Y. Tozuka, Studies in Surface Science and Catalysis 92 (1995) (Sci. Tech. Catal. 1994), 41–50.
[12] A.P. Amrute, C. Mondelli, J. Pérez-Ramírez, Catalysis Science & Technology, 2012. http://dx.doi.org/10.1039/C2CY20185B
[13] K. Seki, K. Iwanaga, T. Hibi, K. Issoh, Y. Mori, T. Abe, Studies in Surface Science and Catalysis 172 (2006) 55–60.
[14] A. Wolf, L. Mleczko, O.F.K. Schlüter, S. Schubert U.S. 2007/0274897 (2007).
[15] A. Wolf, L. Mleczko, S. Schubert, O.F.K. Schlüter, U.S. 2007/0274901 (2007).
[16] A. Wolf, J. Kintrup, O.F.K. Schlüter, L. Mleczko, U.S. 2007/0292336 (2007).
[17] K. Seki, Catalysis Surveys from Asia 14 (2010) 168–175.
[18] D. Teschner, R. Farra, L. Yao, R. Schlögl, H. Soerijanto, R. Schomäcker, T. Schmidt, L. Szentmiklósi, A.P. Amrute, C. Mondelli, J. Pérez-Ramírez, G. Novell-Leruth, N. López, Journal of Catalysis 28 (2012) 273–284.
[19] S. Zweidinger, J.P. Hofmann, O. Balmes, E. Lundgren, H. Over, Journal of Catalysis 272 (2010) 169–175.
[20] C. Mondelli, A.P. Amrute, F. Krumeich, T. Schmidt, J. Pérez-Ramírez, Chemcatchem 3 (2011) 657–660.
[21] H. Over, Journal of Physical Chemistry C 116 (2012) 6779–6792.
[22] C. Mondelli, A.P. Amrute, T. Schmidt, J. Pérez-Ramírez, Chemical Communications 47 (2011) 7173–7175.
[23] A.P. Amrute, C. Mondelli, M. Moser, G. Novell-Leruth, N. López, D. Rosenthal, R. Farra, M.E. Schuster, D. Teschner, T. Schmidt, J. Pérez-Ramírez, Journal of Catalysis 286 (2012) 287–297.
[24] W.F. Maier, K. Stöwe, S. Sieg, Angewandte Chemie International Edition 46 (2007) 6016–6067.
[25] R. Potyrailo, K. Rajan, K. Stöwe, I. Takeuchi, B. Chisholm, H. Lam, ACS Combinatorial Science 13 (2011) 579–633.
[26] A. Holzwarth, W.H. Schmidt, W.F. Maier, Angewandte Chemie International Edition 37 (1998) 2644–2647.
[27] M. Hammes, K. Stöwe, W.F. Maier, Applied Catalysis B 117–118 (2012) 397–405.
[28] J. Scheidtmann, J.W. Saalfrank, W.F. Maier, Studies in Surface Science and Catalysis 145 (2003) 13–20 (Sci Tech. Catal. 2002).
[29] C. Lettmann, H. Hinrichs, W.F. Maier, Angewandte Chemie 113 (2001) 3258–3262.
[30] F.G. Welsch, K. Stöwe, W.F. Maier, ACS Combinatorial Science 13 (2011) 518–529.
[31] B. Wessler, V. Jéhanno, W. Rossner, W.F. Maier, Applied Surface Science 223 (2004) 30–34.
[32] C.C. Chen, M.M. Nasrallah, H.U. Anderson, Journal of the Electrochemical Society 140 (1993) 3555–3559.
[33] J.W. Saalfrank, W.F. Maier, Angewandte Chemie International Edition 43 (2004) 2028–2031.
[34] LabVIEW, Laboratory Virtual Instrumentation Engineering Workbench, v8.2.1, National Instruments, USA, 2007.
[35] TOPAS, General Profile and Structure Analysis Software of Powder Diffraction Data, v2.1, Brucker AXS: Karlsruhe, Germany, 2003.
[36] M.W.M. Hisham, S.W. Benson, Journal of Physical Chemistry 99 (1995) 6194–6198.
[37] P.L. Daniel, R.A. Rapp, Advances in Corrosion Science and Technology, vol. 5, Plenum Press, New York and London, 1975, pp. 68–69.
[38] W. Kangro, R. Jahn, Zeitschrift für anorganische und allgemeine Chemie 210 (1933) 325–336.
[39] S. Kasaoka, Y. Sakata, M. Shirata, Nippon Kagaku Kaishi (1977) 1728–1736.
[40] V. Spitzin, Zeitschrift für anorganische und allgemeine Chemie 189 (1930) 337–366.
[41] T.L. Inyushkina, S.D. Mart'yanova, A.N. Zlobina, Izvestiya Vysshikh Uchebnykh Zavedenii, Tsvetnaya Metallurgiya Translation: Bulletin of the Institutions of Higher Education, Non-Ferrous Metallurgy 17 (1974) 63–67.
[42] V. Tarabanko, N. Tarabanko, N. Koropachinskaya, Catalysis Industry 2 (2010) 259–265.
[43] R. Wasmuht, Angewandte Chemie 43 (1930) 98–101.
[44] A.P. Amrute, C. Mondelli, M.A.G. Hevia, J. Pérez-Ramírez, ACS Catalysis 1 (2011) 583–590.
[45] G.G. Fouga, G. De Micco, A.E. Bohé, Thermochimica Acta 494 (2009) 141–146.
[46] T. Anufrieva, L. Derlyukova, Russian Journal of Inorganic Chemistry 52 (2007) 1840–1843.
[47] S.B. Kanungo, S.K. Mishra, Metallurgical and Materials Transactions B 28B (1997) 371–387.
[48] Y. Ivanshentsev, T.A. Lifant'eva, Izvestiya Vysshikh Uchebnykh Zavedenii, Tsvetnaya Metallurgiya 11 (1968) 20–22.
[49] Y.I. Ivashentsev, V.A. Konakova, Voprosy Khimi i Khimicheskoi Tekhnologii (1968) 90–98.
[50] Y. Ivashentsev, V.A. Konakova, Zhurnal Neorganicheskoi Khimii 12 (1967) 1763–1765.
[51] V.I. Ivashentsev YaI. Ivantsova, Russian Journal of Physical Chemistry 43 (1969) 505–508.
[52] Y. Ivashentsev, V.B. Gerasimova, P.A. Gerasimov, M.I. Dubnyak, E.M. Rechkunova, Izv Vyssh. Ucheb. Zaved., Tsvet. Met. 13 (1970) 79–82.
[53] D. Crihan, M. Knapp, S. Zweidingey, E. Lundgren, C.J. Weststrate, J.N. Andersen, A.P. Seitsonen, H. Over, Angewandte Chemie International Edition 47 (2008) 2131–2134.
[54] Y. Ivashentsev, V.A. Konakova, I.N. Kavitskaya, V.I. Gaivoronskii, Zhurnal Neorganicheskoi Khimii 14 (1969) 64–67.
[55] Y. Ivashentsev, L.I. Kutakova, A.N. Ketov, Izvestiya Vysshikh Uchebnykh Zavedeni Khimiya i Khimicheskaya Tekhnologiya, Translation: Bulletin of the

Institutions of Higher Education, Chemistry and Chemical Technology 11 (1968) 388–391.
[56] V. Lenher, Journal of the American Chemical Society 31 (1909) 243–244.
[57] Y. Ivashentsev, L.I. Kutakova, A.N. Ketov, Voprosy Khimi i Khimicheskoi Tekhnologii (1968) 54–60.
[58] Gmelin, Handbook of Inorganic Chemistry, Springer Verlag, Berlin/Heidelberg/New York, 1982.
[59] J.P. Gaviría, L.G. Navarro, A.E. Bohé, Journal of Physical Chemistry A 116 (2012) 2062–2070.
[60] M.R. Esquivel, A.E. Bohe, D.M. Pasquevich, Thermochimica Acta 398 (2003) 81–91.
[61] G. Aglulin, Kinetics and Catalysis 39 (1998) 521–529.
[62] K. Hachmeister, Zeitschrift fur Anorganische und Allgemeine Chemie 109 (1919) 145–186.
[63] C.C.Y. Chan, D.W. Kirk, Journal of Hazardous Materials 64 (1999) 75–89.
[64] C.W. Arnold, K.A. Kobe, Chemical Engineering Progress 48 (1952) 293–296.
[65] B. Krutzsch, S. Kemmler-Sack, Materials Research Bulletin 19 (1984) 1659–1668.
[66] A.P. Amrute, C.M.A. Mondelli,.G. Hevia, J. Perez-Ramirez, Journal of Physical Chemistry 115 (2011) 1056–1063.